Separation Science and Technology
Publication details, including instructions for authors and subscription information:
http://www.informaworld.com/smpp/title~content=t713708471

Synthesis of Pure Hydroxyapatite and the Effect of Synthesis Conditions on its Yield, Crystallinity, Morphology and Mean Particle Size

N. S. Al-Qasas[a]; S. Rohani[a]
[a] Department of Chemical and Biochemical Engineering, The University of Western Ontario, London, Ontario, Canada

To cite this Article Al-Qasas, N. S. and Rohani, S.(2005) 'Synthesis of Pure Hydroxyapatite and the Effect of Synthesis Conditions on its Yield, Crystallinity, Morphology and Mean Particle Size', Separation Science and Technology, 40: 15, 3187 — 3224
To link to this Article: DOI: 10.1080/01496390500385400
URL: http://dx.doi.org/10.1080/01496390500385400

Separation Science and Technology, 40: 3187–3224, 2005

ISSN 0149-6395 print/1520-5754 online
DOI: 10.1080/01496390500385400

Synthesis of Pure Hydroxyapatite and the Effect of Synthesis Conditions on its Yield, Crystallinity, Morphology and Mean Particle Size

N. S. Al-Qasas and S. Rohani
Department of Chemical and Biochemical Engineering,
The University of Western Ontario, London, Ontario, Canada

Abstract: Hydroxyapatite (HAP) is a calcium phosphate compound with the chemical formula $Ca_5(PO_4)_3OH$. This compound is especially significant in biomedical applications since it resembles the mineral constituents of the hard tissue in the human body. Its biocompatibility, castability, and sinterability make it a very attractive material for simulating bones and therefore for implantations. The objective of this study was to produce HAP with a high purity and to determine quantitatively the exact percentage of HAP in the synthesized powder. Hydrothermal methods have been used to produce HAP. In the present work, Hydroxyapatite powder was produced using the chemical precipitation method in a batch and semi-batch modes of operation. The effect of temperature, pH, and reactant addition rates on the mean particle size was studied. Results showed a maximum in the mean particle size at pH 9, while a minimum was observed at around 45°C. As the reactant addition rate increased the mean particle size increased as well. The purity of the obtained powder was characterized using both quantitative and qualitative techniques. The quantitative results were performed using the powerful Rietveld refinement method. The quantitative results were obtained for three samples. Results showed that pure HAP was produced at a temperature of 85°C, pH 9 and reactant addition rate of 1.3 mL/min.

Keywords: Hydroxyapatite, purity, mean particle size, precipitation, crystallinity, Rietveld refinement

Received 2 February 2005, Accepted 8 September 2005
Address correspondence to S. Rohani, Department of Chemical and Biochemical Engineering, The University of Western Ontario, London, Ontario, Canada N6A 5B9. E-mail: rohani@eng.uwo.ca

INTRODUCTION

The production of different calcium phosphate compounds (here referred to as "phases") has gained significance. The various phases of calcium phosphate have applications in biology, geology, medicine, and dentistry (1). One of these phases that is largely used in biomedical applications is hydroxyapatite (HAP) ($Ca_{10}(PO_4)_6(OH)_2$). The main interest in this phase is due to its similarity to the inorganic component of bones and teeth. Literature published on HAP shows the wide varieties of synthesizing techniques of this compound and many parameters that affect the final product. The system is highly sensitive to preparative solution conditions that lead to the production of the non-stoichiometric hydroxyapatite (ns-HAP). Another problem related to the precipitation of hyrdoxyapatite is the ease of foreign ion incorporation in the lattice of the crystal, which will delay or inhibit the formation of stoichiometric hydroxyapatite (s-HAP). All previous studies showed that amorphous calcium phosphate phase usually precedes the formation of hydroxyapatite. Until now, no one has exactly defined the composition of this amorphous phase. Its structure could vary considerably according to the synthesis conditions and reactant type. The amorphous phase (ACP) could last from a few minutes to 10 hours before it transforms to other phases in the preparative solutions according to the pH and temperature of the system. Also the transformation from the amorphous phase to the crystalline HAP does not usually take place directly. Other crystalline phases could precipitate before HAP. The intermediate phases include octa-calcium phosphate (OCP) and tri-calcium phosphate (TCP). The precipitation of such phases also depends on the initial concentration of the reactants (1). Therefore, production of HAP needs careful control of synthesis conditions. Special care should be taken with regards to the pH and the temperature of the system.

Particle size is an important property in the production of particulate materials. The various applications of specific powders rely on a certain particle size range. Different studies showed very successful results obtained when hydroxyapatite was implanted *in-vivo*.

The various calcium phosphate phases formed in a supersaturated solution in the order of decreasing solubility are: amorphous calcium phosphate (ACP), dicalcium phosphate dihydrate (DCPD), anhydrous calcium phosphate (DCPA), octacalcium phosphate (OCP), tricalcium phosphate (TCP), and hydroxyapatite (HAP). Each phase has its own solubility. Each has its own crystallographical structure (1). The phase of interest, which is hydroxyapatite, is a waxy yellow mineral with hexagonal crystal (2), space group P63/M and lattice parameters $a = 9.424\,Å$, $b = 9.424\,Å$, $c = 6.879\,Å$ and $\gamma = 120^\circ$ (3). Hydroxyapatite crystals are known in their ability for substitution. The OH^- group present in the crystal can be substituted by Cl^- or F^- ions, producing what is known as fluorapatite and chlorapatite. The other ions present in the crystal (PO_4^{+3}, Ca^{+2}) can also be substituted by the various other ions. The solubility of this compound

depends on the synthesis conditions, especially the pH of the solution. The solution compositions also affect the stability of different phases present in the solution. Therefore the production of this phase can be accomplished through variety of ways and methods. The most common synthesis technique is the chemical precipitation and sol-gel.

Eanes et al. (4) produced HAP using aqueous precipitation method at pH 10.5 and temperature of 25°C using high initial concentration of the reactants. The X-ray diffraction (XRD) and chemical analysis method were used for the product characterization. Results showed that the first phase to precipitate was an amorphous phase, and they could recognize 3 stages. The first stage began once mixing started and lasted for 5 hours; it was mainly an amorphous like material. The second stage was the gradual transformation from the amorphous phase to a poorly crystalline phase. The third stage was the development of a fully crystalline phase and it was characterized by the constancy of the (002) peak area. The last stage occurred at around 7 hours after the reaction was initiated. At the beginning of the second stage, 20% of the amorphous phase was converted to a crystalline phase, while the balance (80%) was converted during the last stage. This showed that the conversion proceeds faster after the second stage. The (002) peak kept constant till the end of the second stage, which suggests that the rate of conversion of the amorphous phase in stage two depends on the nucleation of new crystals and not on the growth of pre-existing crystals. The third stage was distinguished with the high increase of crysallinity. A reprecipitation process was also observed at this stage. The calcium ion concentration was decreased from 0.42 to 0.2 mg/mL in the solution, indicating the uptake of calcium ion from the solution.

Boskey and Posner (5) studied the formation of HAP from amorphous Phase at a constant temperature as a function of pH. Several experiments were conducted at pH 6.8, 7, 7.5, 8, 9 and 10. The transformation from amorphous to crystalline HAP was detected by XRD. Results showed that at all pH values there were three distinct regions. Induction period, where there is no change in the extent of reaction, then the proliferation period, which is characterized by a rapid increase in the extent of reaction per unit time, and finally the tapering off period, where the conversion becomes constant or increases at a slow rate. The induction period was found to increase as the pH increased. Other factors that decreased the induction period included smaller ACP particles, higher ACP slurry concentration, lower pH, and a higher temperature. The increase in the transformation rate at higher temperatures is due to the increasing ACP solubility and the addition of energy, which accelerate the formation of HAP nuclei. Other factors found to affect the conversion were the stirring rate and the concentration of the reactants in solution. The induction period was much smaller at higher temperatures.

Meyer and Eanes (6) studied the structure and composition of ACP and the main factors that influence its transformation to a crystalline phase. The

experiments were run under a wide range of conditions in order to investigate the factors affecting the thermodynamic behavior of the phase transitions. They showed that the amorphous calcium phosphate molecular formula could be best described as TCP like phase. Also they showed that the ACP solubility decreases rapidly with increasing pH. TCP's ionic product varies little over a range of pH from 7.4 to 9.25. While the ionic product of HAP, OCP and DCPD increase greatly with increasing pH. Another set of experiments was carried out at various reactants Ca/P ratios. Percentage of HAP in the product increased as this ratio increased, while the opposite happened for OCP and DCPD. Meyer and Eanes were able to prove that the precipitation of the crystalline phase occurs by a heterogeneous nucleation step on the exterior of the pre- formed amorphous phase. Also they distinguished 3 regions during the precipitation. The first one was the precipitation of the amorphous phase that had a structure similar to TCP. The second one was accompanied by the nucleation of an OCP-like phase. Finally the third stage corresponded to the formation of a crystalline apatitic structure, which in turn converted to HAP.

Harries et al. (7) studied the conversion of amorphous calcium phosphate to crystalline HAP using the chemical precipitation method. They used the Extended X-Ray Absorption Fine Structure (EXAFS) method, in addition to the XRD and infrared (IR). The EXAFS has the advantage that it can define radial distribution functions. Thus it can elucidate the degree of order in the powder, which in turn gives an indication about the crystallinity of the product. At $pH = 10$, $T = 20^{\circ}C$ and low concentration of reactants; a poorly crystalline HAP was produced after around 120 hours. The XRD patterns and IR spectra showed a poor crystalline powder that started to form after 19 hours and finally transformed to a more crystalline phase after 22 hours. Any further maturation of the solution did not lead to a significant increase in the crystallinity at these preparative conditions.

A study done by Kivrak and Tas (8) showed that a composite material consisting of both HAP and TCP can be used to simulate the human bones. Aqueous solutions of $Ca(NO_3)_2$ and $(NH_4)_2HPO_4$ were used as the starting materials. They produced a composite material containing different HAP and TCP concentrations. Each sample was heated to different temperatures (1000, 1100, 1200, and 1300°C). They found that the phase distribution of HAP and TCP in the composite material relies on the synthesis temperature. The final results showed that the composite material that contains more or equal to 60% HAP, was suitable to manufacture calcium phosphate bioceramic implants.

Seckler et al. (9) conducted a semi-batch experiment to produce hydroxyapatite. They maintained the temperature at 90°C and used a slow addition rate of reactant to keep a low supersaturation in the system. They mainly studied the effect of supersaturation on the quality of the HAP produced by varying the reactant concentration, reactant addition rate, temperature and pH. Also they studied the effect of carbon incorporation on the

HAP. The reactants used were ammonium acetate solution, calcium nitrate solution, diammonium phosphate solution and ammonium hydroxide solution. The pH was adjusted to 8.5–9. Results showed that longer reactant addition time results in a better crystallinity of HAP. The temperature effect was also clear in their results. At room temperature the main phase that had been produced was ACP while at 90°C the main phase was HAP. This is attributed to the increase in the HAP solubility at lower temperature. The pH affects the crystallinity and the size of the crystals. The highest crystallinity and the nano-size crystals were formed at higher pH values. Seckler et al. related the crystallinity of the produced powder to the concentration of the NH_4OH solution added. At a lower concentration the crystals showed higher crystallinity.

Rodriguez-Lorenzo and Vallet-Regi (10) conducted several experiments to produce apatites with a different stoichiometry and morphology. The effect of synthesis conditions was recorded. The main parameters that were affected by the synthesis conditions were crystallinity and morphology. The reagents that were used in the experiments were calcium nitrate, ammonium phosphate, and ammonium hydroxide. The reagents were added simultaneously at a flow rate of 22 mL/min. The produced powders were washed and then dried at a temperature of 104°C. The reagent concentration, reactor temperature, solution pH, reaction time, aging time, and finally the atmosphere within the reaction vessel were all varied in order to study their effect on the final product. The reactant concentrations did not show a dramatic influence on the characteristics of the obtained powder. An increase in the temperature decreased the maximum width of the XRD peaks, showing bigger coherent diffraction domain at higher temperatures. Also the surface area of the particles decreased with increasing the temperature. The increase in the reaction time increases the Ca/P ratio; also longer reaction time produced bigger crystals. Lower pH produced powders with lower Ca/P ratios and smaller crystal size. Different atmospheres were examined. Synthesis under CO_2 conditions, promoted the incorporation of CO_3^{-2} ion in the HAP lattice. The XRD pattern showed a decrease in the crystallinity for samples synthesized under CO_2 atmosphere, and this was because of the formation of carbonated apatite. The N_2 atmosphere showed the presence of nitrates, which came from the calcium nitrate reagents used.

Salahi and Moztarzadeh (11) studied the composition of calcium phosphates precipitated from aqueous solution at different pH values. They used $Ca(NO_3)_2$ and $(NH_4)_2HPO_4$ as the reagents. The calcium solution was introduced first in the reactor and stirred vigorously at 20°C. The phosphate solution was added drop by drop for 60 min. The product was centrifuged and dried at a temperature of 50°C for 15 hours. The inductively coupled plasma technique, XRD, IR, and scanning electron microscope (SEM) were used to characterize the produced sample. Results showed a crystalline structure of DCP ($CaHPO_4$) at pH 6–8. A by-product was formed which was NH_4NO_3. At pH ranging from 8–10, results of both XRD and IR

showed the presence of HAP. Clear bands of PO_4^{-3} and OH^{-1} were observed in the IR analysis. Over the pH range 4–8, a Ca/P corresponding to DCP and DCPD was observed. However at pH 7, 8, and 9 the Ca/P ratio increased to 1.3, which corresponds to the amorphous calcium phosphate. At pH 10 this ratio reached 1.5, which showed the presence of calcium deficient hydroxyapatite.

Liu et al. (12) studied the kinetics and formation of hydroxyapatite at pH 10–11 and 0.5 M calcium ion concentration. The aim was to investigate the transformation of OCP to HAP in the pH range of 10–11. It was found that OCP is a transitional phase that is formed before HAP particles appear. Initial reactants of 1 mol/L of Ca $(NO_3)_2$ and 1 mol/L of $(NH_4)HPO_4$ were mixed with Ca/P ratio more than 1.67. Samples at different intervals were taken. These samples were washed, filtered, and dried. The sample characterization was performed using Fourier Transform Infrared spectroscopy (FTIR), and X- Ray Powder Diffraction (XRD). The samples were treated at a temperature of 800°C for phase transition and then analyzed on the XRD. The kinetics of the reaction was determined by varying the reaction temperature. The reaction time and Ca/P ratio were measured for each run. Subsequently the conversion rates were obtained for each run. Their results showed that the Ca/P ratio at 35°C was less than 1.5 initially. It then increased with time until it reached a value of 1.67 after a long period of time. The FTIR results indicated that OCP was present at the beginning and then transformed to amorphous calcium phosphate very quickly. The ACP phase was transformed to TCP after heat treatment and finally a mixture of HAP and TCP was obtained. The results showed that the temperature of the reaction influenced the reaction rate. As the reaction temperature increased, the formation of HAP accelerated. It was found that HAP could be formed after around 24 hours at room temperature while it just took 5 min at 60°C. Also the temperature was found to affect the morphology of HAP. For example at 15°C, the particle size was less than 10 nm, while at 60°C it was around 100 nm. The presence of crystal seeds was thought to affect the particle size and shape. To prepare small particles, more reaction time was needed. A kinetics study was conducted and the reaction rate law of the transformation of OCP to HAP was obtained. The activation energy was found to be 95 kJ/mol. A diffusion-controlled process was suggested for this process.

Torrent-Burgues and Rodriguez-Clemente (13) studied the precipitation of hydroxyapatite in aqueous solution at 85°C in a semi-batch reactor. They recorded the influence of pH, reactant addition and flow rates on the stoichiometry and crystallinity of the product. The experiments were conducted in a thermosted reactor at a temperature of 85°C. $CaCl_2$ and K_2HPO_4 were used as the reagents and KOH was added to adjust the pH of the system. The product was analyzed using IR spectroscopy and XRD. The Ca/P ratio was determined using induced plasma atomic absorption, besides the images that were obtained with a transmission electron microscope (TEM). Results showed that the reactant addition order controlled the yield of the product

and its Ca/P ratio. As K_2HPO_4 was added to $CaCl_2$, a stoichiometric apatite was formed with Ca/P ratio of 1.67. While when $CaCl_2$ was added to K_2HPO_4, a non-stoichiometric apatite formed with Ca/P ratio of 1.53. Also the reactant addition order affected the crystallinity of the final product. The mean crystal size was estimated from the diffractograms and Scherrer formula.

$$D = k\lambda/B_{12}\cos\theta \tag{1}$$

$$\beta_{1/2} = (B^2 - b^2)^{1/2} \tag{2}$$

where k is the shape factor, λ is the wavelength of X-rays, θ is the diffraction angle, B is the diffraction peak width at half height and b is the natural width of the instrument. The TEM micrographs showed nanosized needle like crystals. The rate of addition did not affect the stoichimetry of the product or its crystallinity.

Petrov et al. (14) produced calcium phosphate cement by combining HAP with alfa and beta TCP. They examined the preparation of Ca-P bi-phase using calcium phosphate precipitate. The powders were sintered at different temperatures for different time intervals. The powders were precipitated at pH = 11.5, and temperature of 20°C. The product was sintered at 450, 800, 1050, and 1200°C. The characterization of the samples was carried using XRD, SEM and TEM. The samples were left to age for 24 hours. The XRD patterns showed a broad peak corresponding to HAP. They noticed two stages in the formation of HAP crystals, the first one was the amorphous formation and the second one was the crystal formation that happened after a certain induction time. This result is consistent with all of the above studies. Analysis showed that the powder was a non-stoichiometric HAP. The Ca/P was found to be 1.47 after treating the sample at a temperature of 90°C.

Shuk et al. (15) prepared HAP powder at room temperature from heterogeneous reaction. They used $Ca(OH)_2$ powder and $(NH_4)_2HPO_4$ solution to produce a stoichiometric HAP via the mechanochemical–hydrothermal method. The mechanochemical-hydrothermal method, not like the mechanochemical method that involves only solid-state reaction, takes advantage of the presence of an aqueous solution in the system as well. This method is in between the mechanochemical and hydrothermal methods. The mechanochemical–hydrothermal route is able to produce HAP powders with a yield similar to the hydrothermal processes but it does not require a high temperature. Shuk et al. argued that the previous methods to produce HAP were not able to produce a good crystalline HAP with a Ca/P ratio ranging from 1.5–1.64 (non-stoichiometric HAP). The calcination procedure stimulates the presence of TCP phase besides the HAP phase. Therefore the aim of this study was to produce a stoichiometric and well-crystalline HAP powder using the mechanochemical-hydrothermal method. The mechanochemical-hydrothermal method was accomplished by placing slurries into a laboratory

scale mill. The grinding was done in the air initially at a rotation speed of 1500 rpm for 1 hour and then at 800 rpm for 4 hours. During grinding the temperature was monitored. They used XRD, FTIR, field emission scanning electron microscopy (FESEM), and thermogravimetric analysis to study the produced powders. The XRD patterns showed only peaks related to HAP phase, and no other phase was detected. The heat-treated powders at 900–1100°C showed narrow XRD patterns. Samples heat-treated at 1100°C showed the presence of low intensity peaks attributed to β-TCP. The Ca/P ratio was around 1.76, which is very close to the theoretical value of HAP. The FTIR spectrum revealed the presence of the characteristics peaks of HAP. Carbonate ions were found at 870 cm^{-1} and 1420–1480 cm^{-1}. Low intensities of OH^{-1} bands were also located in the spectrum. This low intensity was attributed either to the large specific surface area of the HAP powders, the presence of absorbed water, or the incorporation of some carbonate ions in the HAP lattice. Thermogravimetric analysis of the non-heat treated powder showed a weight loss up to 450°C; this is due to the loss of absorbed water and lattice water. The powder had a very small crystal size ranging from 20–21 nm. The FESEM showed the presence of agglomerates that consisted of very tiny crystals. They finally emphasized the importance of the aqueous solutions in the preparation of HAP. It participates in the synthesis reaction via dissolving one of the reactant. This is an advantage over the conventional mechanochemical synthesis.

Gomez-Morales et al. (16) conducted a study similar to Burgues and Rodriguez-Clemente (2001), but with a continuous mixed-suspension mixed product removal (MSMPR) reactor. This experiment was conducted at 85°C and pH 9, with N_2 addition. K_2HPO_4, and $CaCl_2$ were used as reactants and KOH to control the pH of the system. The concentrations were adjusted in a way to keep the Ca/P ratio fixed to 1.67. Different residence times were used in different runs, which were accomplished by changing the flow rates of the reactants. Another run was conducted by replacing $CaCl_2$ by $Ca(NO_3)_2$. Different characterization techniques were used such as XRD, IR, coupled plasma atomic spectroscopy and finally the transmission electron microscope. The particle size distribution was analyzed as well. This work showed the effect of residence time on the crystalline phase, Ca/P ratio, the yield, production rate, and the average size of the particles. Generally in all runs the yield was found to be more than 80%. It was found also that the production rate increased as the reagent concentration increased, and decreased with the increase of residence time. The crystal shape was needle like with an average size of 1.5 μm. The average crystal size was calculated using Scherrer equation. The crystallinity index was also determined using the following relation:

$$X(\%) = \frac{P/p}{(P/p)_{ref}} \times 100 \tag{3}$$

where P is the height of the diffraction peak, P/p and $(P/p)_{ref}$ are the ratios of the total coherent scattering to the background for a given sample for the standard substance, respectively. The crystallinity index of human enamel apatite is 60% and of bone and dentine is 35%. This work showed that the produced crystals have a crystallinity index very close to bone and dentine apatite. An important conclusion was reached to show that when $Ca(NO_3)_2$ is used as a reagent instead of $CaCl_2$, the transformation of ACP is much slower than using the other reagent. Finally Gomez-Morales et al. revealed that the high temperature enhances the transformation from ACP to HAP.

Kim et al. (17) studied the effect of operating conditions on the crystalline properties of HAP powder in a semi-batch reactor. The powder was prepared by reaction crystallization of $CaCl_2$, KH_2PO_4, and NaOH solution. The ratio between $CaCl_2$ and KH_2PO_4 was kept constant at the value of 1.67. The $CaCl_2$ solution was introduced to the reactor that contained the NaOH and KH_2PO_4 solution within one hour. The temperature was adjusted to 60°C. The powder was kept in the reactor for 5 hours and then filtered using 0.45 μm pore size filter paper and dried for one hour at a temperature of 50°C. The synthesis powder then was analyzed using XRD. Before starting the reaction, Kim et al. studied the change in pH with different concentration of NaOH and KH_2PO_4. They found that the pH of the mixture solution always exceeded 12 when NaOH was added in excess of twice or more than KH_2PO_4. They concluded that KH_2PO_4 was totally ionized to PO_4^{-3}. This will help avoid the production of any by products. The XRD patterns showed similarity to the standard HAP profile. The crystalline properties such as relative crystallinity and grain size were obtained from the XRD graph. They showed that the relative crystallinity is affected by OH^- concentration. It decreased as the OH^- ion concentration increased. The size of the crystals was affected by OH^- ion concentration as well. As the OH^- ion concentration increased, pH increased, and the size of the crystals decreased. This means that the nucleation was favored at high OH^- ion concentration or higher pH values. While the growth was favored at lower OH^- ion concentration or lower pH values.

Sarig and Kahana (18) produced nano-crystals of hydroxyapatite of approximately 300 nm. They used the precipitation method using calcium chloride and sodium phosphate as the starting reagents. The experiment was run at room temperature and a pH of 7.4. The precipitation of calcium phosphate was achieved by subjecting the aqueous solution to microwave irradiation immediately after mixing. According to their results they proved that the produced crystals had a great advantage because they were in nano-size range and at the same time they were aggregated in small spherulites with an open and a loose structure. This helped in storing the powder for a long period (3 years as mentioned in this study). The powder produced by this method was bouncy and free-flowing. The use of microwave helped in achieving rapid crystallization, which in turn produced very small crystals.

Raynaud et al. (19) produced a calcium phosphate precipitate with a Ca/P ratio in the range of 1.5–1.667 and studied its thermal stability. They

produced a powder by a conventional aqueous precipitation method. The powder was analyzed using XRD, IR, and SEM. They arrived at the conclusion that the production of calcium phosphate phases within the above range of Ca/P ratios needs good regulation of operating conditions such as pH and temperature. Raynaud et al. synthesized powders using different initial Ca/P ratios. The first powder with an initial Ca/P ratio in the range $1.5 < Ca/P < 1.667$, the second one was synthesized using an initial $Ca/P < 1.5$, third one with Ca/P ratio $= 1.667$ and the last one with $Ca/P > 1.667$. The XRD patterns for powder with an initial Ca/P ratio in the range of 1.5–1.667 showed patterns very similar to HAP pattern but with very broad peaks, which indicated the low crystallinity of the powder. Powders synthesized using initial $Ca/P < 1.5$, showed the presence of two crystalline phases corresponding to HAP and monetite structure. The one synthesized at $Ca/P = 1.7$ showed HAP pattern without the presence of any other phases. The FTIR results agreed with the XRD. The main phosphate bands were detected in addition to the OH^{-1} and some carbonate bands. A band at $875\,cm^{-1}$ was attributed to HPO_4^{-2} or NO_3^-. The presence of HPO_4^{-2} is an indication of deficient hydroxyapatite (Ca-dHAP). Bands at 1380 and $820\,cm^{-1}$ were assigned to some residual nitrate groups. After heat treatments at 600°C, these residual bands disappeared completely, while the one at $875\,cm^{-1}$ remained. At 400°C, band at $720\,cm^{-1}$ was attributed to the pyrophosphate groups. It disappeared when heating to 1000°C for powders with initial Ca/P from 1.5–1.667. This revealed the condensation of hydrogenophosphate groups in Ca-dHAP in the range 350–720°C. For $Ca/P < 1.5$ several bands at 720, 920, and $1200\,cm^{-1}$ assigned for pyrophosphates were still present at 1000°C and the band at $630\,cm^{-1}$ disappeared. This revealed the conversion of $CaHPO_4$ to $\beta-Ca_2P_2O_7$ and the dehydroxylation of apatitic TCP to $\beta-Ca_3(PO_4)_2$. The powder synthesized at $Ca/P = 1.667$ showed stability when heated to elevated temperatures. CaO was detected at 750°C, which suggested the presence of $Ca(OH)_2$.

Koumoulidis et al. (20) prepared a calcium phosphate powder using a precipitation method known as "pH shock wave method". It involves a rapid increase in the pH value by adding concentrated NH_4OH solution. The reagents that had been used were $CaCl_2$ and $Ca(H_2PO_4)_2 \cdot H_2O$. The temperature was adjusted to 97°C and the pH was increased rapidly from 3.22 to 8.79. A powder was produced and aged at the above conditions for 30 min. Some of the prepared powders were calcined at 550, 800, and 1400°C. The characterization of the sample was performed using XRD, FTIR, TEM and textural studies were performed by nitrogen adsorption porosimeter. The results showed that they had produced a non-stoichiometric hydroxyapatite with Ca/P ratio equal to 1.477. The XRD pattern showed strong peaks corresponding to crystalline HAP. While the lattice parameters were found to differ from those for the standard card and that was related to HPO_4^{-2} group. The high degree of crystallinity of the produced powder was thought to be due to the rapid increase of pH, which resulted in a supersaturated

HAP solution. The crystal size was found to be in the range of 14.9–31 nm. The calcined powders at 550, 800, and 1400°C were analyzed in the FTIR. The FTIR results showed a broad band at 3100–3500 cm^{-1} corresponding to the adsorbed hydrate. This band was found to decrease as the temperature increased. A peak at 868 cm^{1} corresponding to P–O–H was found and this indicated the presence of HPO_4^{-2} group, which in turn showed that a non-stoichiometric HAP had been formed. Also a PO_4^{-3} peak was found at 473, 564, 602, 962, 1033, and 1093 cm^{-1}. A sharp peak of O–H was found at 663 cm^{-1}, indicating the presence of HAP phase. This peak was decreased gradually as the calcination temperature increased and it disappeared totally at 1400°C. The TEM results showed that the particle average size was in the range of 80–200 nm in length and 10–30 nm in width. They formed aggregates with an average diameter of 1–5 μm.

Saeri et al. (21) studied the effect of heating and aging time on the morphology and crystallinity of the powders. They precipitated hydroxyapatite using the wet chemical method. They used orthophosphoric acid and calcium hydroxide as the initial reagents. The reaction was run at 40°C and pH 7.5. The reaction concentration was 0.3 M and 0.5 M for the orthophosphoric acid and calcium hydroxide, respectively. Three samples were prepared to study the effect of time. The first one was prepared from the fresh precipitate, after two hours the second sample was prepared. Then the solution was washed with degassed distilled water and the third sample was separated. All precipitations were further washed and left overnight. Final sample (Sample 4) was washed and then dried at 80°C overnight. All samples were then characterized using XRD, FESEM, and Raman spectroscopy. The FESEM images for samples one, two, and three had almost the same morphology with rod-like or long plate-like crystals. Only sample 3 showed coarse morphology indicating more growth. The images showed also that the crystals tended to form small agglomerates. Sample 4 showed a mean size of 1 μm also hollow spaces between the particles were observed. These samples underwent a heat treatment at 850 and 1200°C for 2 hours. The XRD patterns for the as-prepared powder and the heat-treated ones, revealed an HAP pattern for all the samples but with higher crystallinity at 850°C. The crystallinity decreased after heating at 1200°C. Raman spectroscopy showed the disappearance of OH^{-1} band for the sample synthesized at 1200°C, which is in agreement with the XRD results. No other phase was observed in the heat-treated samples.

Arifuzzaman and Rohani (22) studied the effect of initial calcium concentration and the volume mean diameter as a function of pH. The work was done in a batch reactor and at 25°C and pH below 7.1. Several initial concentrations were employed. The final powder was characterized using FTIR and XRD. Results revealed the presence of brushite (dicalcium phosphate dihydrate) as the main phase. The only other phase detected was amorphous calcium phosphate that precipitated at a pH higher than 6.8. The nucleation pH was found to vary with the initial concentration. Higher initial concentrations

promoted nucleation at lower pH. No significant effect of initial concentration on the volume-weighted mean was noticed during their experiments. Similarly the span and the mean crystal size showed no large dependency on the initial calcium and phosphate concentrations. The morphology of the obtained crystals was plate-like as indicated by the SEM images.

In the present study, hydroxyapatite was produced using a chemical precipitation method in both batch and semi-batch modes of operation. It offers a fast and easy way to produce most pure hydroxyapatite. The conditions and the procedures used in this study were deduced from the above literature. The aim was to produce a high purity hydroxyapatite and to study the different factors that affect its production. Crystallinity (23) determines the degree of the order of the atoms in the lattice. Dislocations, vacancies, defects, shear planes, thermal expansion, and contractions can all reduce crystallinity.

Although HAP has been synthesized using different methods and techniques, the production and the different factors affecting the final characteristics and compositions of the powder are still not fully optimized. Among the problems encountered is the ability to characterize and examine the purity of the final product. The production of HAP powder with high purity and a desired particle size determines the type of application of the produced powder.

MATERIALS AND METHODS

Hydroxyapatite particles were prepared by chemical precipitation from an aqueous solution. Calcium chloride and sodium phosphate monobasic monohydrate were used as the reagents. Different concentrations of the starting materials were prepared. The Ca/P ratio of 1.67 was maintained in all cases. During each experiment the temperature and pH were kept constant. The experimental apparatus consisted of a reactor with heating jacket, pH controller, heating and circulating bath and pumps. Figure 1 shows a schematic diagram of the experimental set up. The jacketed reactor used in the experiment was a 3-liter cylindrical Pyrex glass reactor supported by a stainless steel frame. The reactor was round-bottomed with four wall baffles. The impeller was a marine type impeller with helical pitch located at the center of the reactor. A 115 V Fisher Scientific motor with a DC speed motor controller was used to drive the shaft. The upper stainless steel lid contained several connections to allow the addition of reactants, NaOH, HCl and N_2 gas supplement. A 0.265 in. tube was inserted inside the reactor where the reactants were pumped through it. It was located 1 in. from the inner wall of the reactor and 6 in. below the liquid level. The NaOH and HCl solutions were pumped to the reactor approximately in the center of the reactor as shown in Fig. 2.

The reactants were heated to the desired temperature and then added to the reactor with rapid mixing under nitrogen gas. The pH was controlled by

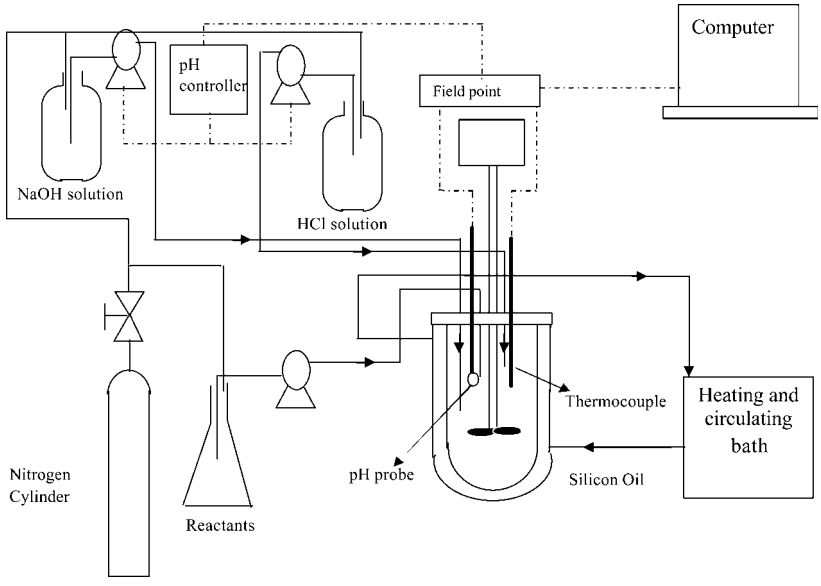

Figure 1. The experimental setup.

adding either NaOH or HCl. All the data from the thermocouple, pH meter, and turbiditimeter were sent to a labView program through a field point. The impeller speed and the feed location were kept constant for the entire study. Since HAP is known to be thermodynamically the most stable calcium phosphate, each experiment was run for 8 hours to ensure that the final precipitate will be HAP; some experiments lasted only for 4 hours. During the feed preparation and in all the experiments, the feed tanks and the reactor were purged with a stream of nitrogen gas in order to avoid carbonate precipitation (please see Fig. 1). More than 50 experiments were conducted at different conditions. Table 1 shows the set of runs and the conditions. The reaction of HAP formation is as follows

$$5CaCl_2 + 3NaH_2PO_4 + 7NaOH \rightarrow Ca_5(PO_4)_3OH + 10NaCl + 6H_2O \qquad (4)$$

In order to study the effect of the various operating conditions on the mean particle size of HAP, different concentrations of the reactants were prepared. Two concentrations were used in this study, 0.01 and 0.05 M for the Ca^{+2} ion concentration and 0.03 and 0.006 M for the PO_4^{-3} ions. The ratio of 1.67 was maintained in both cases. Several sets of experiments were run at different temperatures, during each run both the temperature and pH were kept constant. Five temperatures were used: 25, 44, 55, 60 and 85°C. Three sets of experiments were conducted to study the temperature effect. Each set consisted of 5 experiments. Each run was at a different

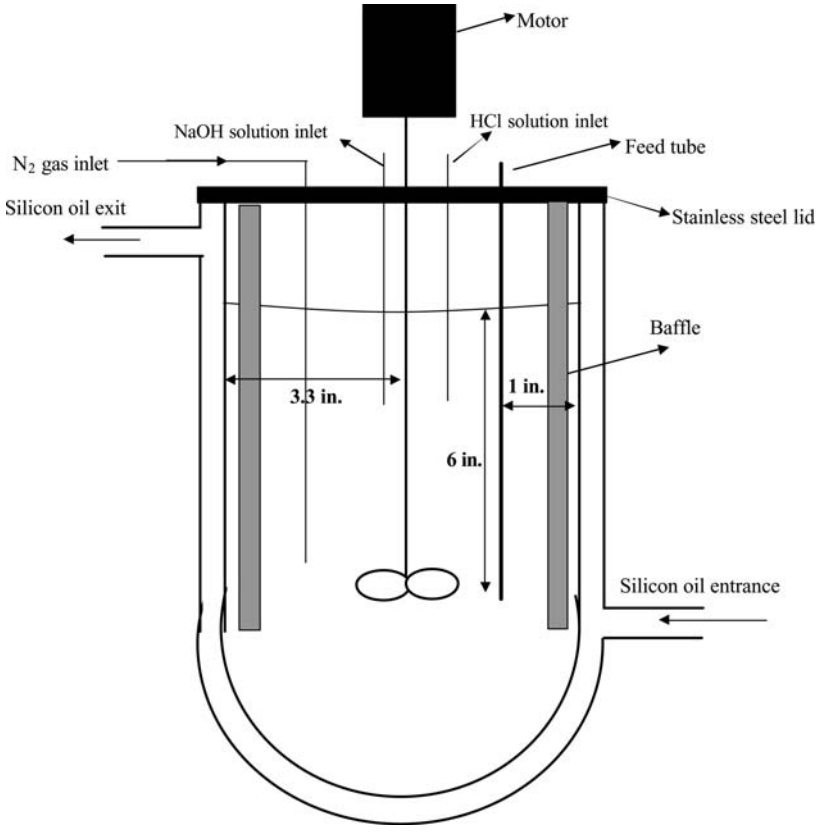

Figure 2. A schematic diagram of the crystallization reactor.

temperature while all the other parameters were kept constant. For all experiments in this set, the stirring rate and the rate of reactant addition were kept constant at 350 rpm and 3 mL/min, respectively. Most of the experiments were performed in semi-batch mode, with different reactant addition order (either Ca^{+2} ions added to PO_4^{-3} ions or vice versa). One set of experiments was run in a batch mode. Table 2 shows the conditions of the experiments. The effect of pH was studied at pH 7, 8, 9, 10 and 11. Three sets of experiments were run; each set consisted of 5 experiments. Set one was conducted at 85°C and at a calcium ion concentration equal to 0.01 M, set two at 25°C and calcium ion concentration equal to 0.05 M, and the third set was conducted at 85°C and calcium ion concentration equal to 0.05 M (Table 3). A third series of experiments was performed to study the effect of reactant addition rate (AR) on the particle size. This series contained two sets of experiments; each with 4 runs at different reactants addition rates. Table 4 lists all experiments in this series.

Table 1. List of experiments ran at various synthesis conditions

Exp. no.	T (°C)	pH	RAO	$[Ca^{2+}]$ (M)	$[PO_4^{-3}]$ (M)	t_f (hr)	AR (mL/min)
Exp. 7	25	9	PO_4^{-3} added to Ca^{2+}	0.01	0.006	8	3
Exp. 8	25	9	Both in the reactor	0.01	0.006	8	3
Exp. 9	25	9	Ca^{2+} added to PO_4^{-3}	0.01	0.006	8	3
Exp. 10	85	9	PO_4^{-3} added to Ca^{2+}	0.01	0.006	8	3
Exp. 11	85	9	Both in the reactor	0.01	0.006	8	3
Exp. 12	85	9	Ca^{2+} added to PO_4^{-3}	0.01	0.006	8	3
Exp. 13	25	9	PO_4^{-3} added to Ca^{2+}	0.05	0.03	8	3
Exp. 14	25	9	Both in the reactor	0.05	0.03	8	3
Exp. 15	25	9	Ca^{2+} added to PO_4^{-3}	0.05	0.03	8	3
Exp. 16	85	9	PO_4^{-3} added to Ca^{2+}	0.05	0.03	8	3
Exp. 17	85	9	Both in the reactor	0.05	0.03	8	3
Exp. 18	85	9	Ca^{2+} added to PO_4^{-3}	0.05	0.03	8	3
Exp. 19	85	7.4	PO_4^{-3} added to Ca^{2+}	0.05	0.03	8	3
Exp. 20	25	11	PO_4^{-3} added to Ca^{2+}	0.05	0.03	8	3
Exp. 21	85	9	PO_4^{-3} added to Ca^{2+}	0.05	0.03	4	3
Exp. 22	25	9	PO_4^{-3} added to Ca^{2+}	0.05	0.03	4	3
Exp. 23	85	9	PO_4^{-3} added to Ca^{2+}	0.01	0.03	4	3
Exp. 24	25	9	PO_4^{-3} added to Ca^{2+}	0.01	0.03	4	3
Exp. 25	25	9	PO_4^{-3} added to Ca^{2+}	0.007	0.0042	8	3
Exp. 26	25	9	Both in the reactor	0.007	0.0042	8	3
Exp. 27	25	9	Ca^{2+} added to PO_4^{-3}	0.007	0.0042	8	3
Exp. 28	25	9	PO_4^{-3} added to Ca^{2+}	0.01	0.006	8	0.8
Exp. 29	85	9	PO_4^{-3} added to Ca^{2+}	0.01	0.006	8	0.8

(*continued*)

Table 1. Continued

Exp. no.	T (°C)	pH	RAO	$[Ca^{2+}]$ (M)	$[PO_4^{-3}]$ (M)	t_f (hr)	AR (mL/min)
Exp. 31	85	11	PO_4^{-3} added to Ca^{2+}	0.01	0.006	8	3
Exp. 32	85	7.4	PO_4^{-3} added to Ca^{2+}	0.01	0.006	8	3
Exp. 33	85	9	PO_4^{-3} added to Ca^{2+}	0.01	0.006	8	1.3
Exp. 34	85	9	PO_4^{-3} added to Ca^{2+}	0.01	0.006	4	0.8
Exp. 36	85	11	PO_4^{-3} added to Ca^{2+}	0.05	0.03	8	3
Exp. 37	25	7.4	PO_4^{-3} added to Ca^{2+}	0.05	0.03	8	3
Exp. 38	25	11	PO_4^{-3} added to Ca^{2+}	0.05	0.03	8	3
Exp. 39	25	9	PO_4^{-3} added to Ca^{2+}	0.01	0.006	8	1.3
Exp. 41	85	9	PO_4^{-3} added to Ca^{2+}	0.007	0.0042	8	3
Exp. 42	60	9	Ca^{2+} added to PO_4^{-3}	0.01	0.006	8	3
Exp. 43	44	9	Ca^{2+} added to PO_4^{-3}	0.01	0.006	8	3
Exp. 44	85	8	PO_4^{-3} added to Ca^{2+}	0.01	0.006	8	3
Exp. 45	25	8	PO_4^{-3} added to Ca^{2+}	0.05	0.03	8	3
Exp. 46	85	10	PO_4^{-3} added to Ca^{2+}	0.01	0.006	8	3
Exp. 47	25	10	PO_4^{-3} added to Ca^{2+}	0.05	0.03	8	3
Exp. 48	60	9	Both in the reactor	0.01	0.006	8	3
Exp. 49	44	9	Both in the reactor	0.01	0.006	8	3
Exp. 50	60	9	PO_4^{-3} added to Ca^{2+}	0.05	0.03	8	3
Exp. 51	44	9	PO_4^{-3} added to Ca^{2+}	0.05	0.03	8	3
Exp. 52	55	9	Both in the reactor	0.01	0.006	8	3
Exp. 53	55	9	Ca^{2+} added to PO_4^{-3}	0.01	0.006	8	3
Exp. 54	55	9	PO_4^{-3} added to Ca^{2+}	0.05	0.03	8	3
Exp. 55	25	9	PO_4^{-3} added to Ca^{2+}	0.01	0.006	8	3
Exp. 56	85	9	PO_4^{-3} added to Ca^{2+}	0.01	0.006	8	3

RAO: reactant addition order, AR: addition rate.

Table 2. Experiment sets ran to study the effect of temperature

Set no.	Exp. no.	T (°C)	$[Ca^{2+}]$ mol/L	RA mL/min	pH	RAO
1	Exp. 8	25	0.01	3	9	Both in the reactor
	Exp. 49	44				
	Exp. 52	55				
	Exp. 48	60				
	Exp. 11	85				
2	Exp. 9	25	0.01	3	9	Ca^{2+} added to PO_4^{-3}
	Exp. 34	44				
	Exp. 53	55				
	Exp. 42	60				
	Exp. 12	85				
3	Exp. 13	25	0.05	3	9	PO_4^{-3} added to Ca^{2+}
	Exp. 44	44				
	Exp. 54	55				
	Exp. 50	60				
	Exp. 16	85				

RAO: reactants addition order, RA: reactants addition rates.

CHARACTERIZATION

To characterize the synthesized powder, both qualitative and quantitative techniques were used. The qualitative techniques were performed using FTIR, SEM, EDX, and XRD. The FTIR and XRD were used to study

Table 3. Experiment sets ran to study the effect of pH

Set no.	Exp. no.	pH	$[Ca^{2+}]$ mol/L	RA mL/min	T (°C)	RAO
1	Exp. 32	7	0.01	3	85	PO_4^{-3} added to Ca^{2+}
	Exp. 44	8				
	Exp. 10	9				
	Exp. 46	10				
	Exp. 31	11				
2	Exp. 37	7	0.01	3	25	PO_4^{-3} added to Ca^{2+}
	Exp. 45	8				
	Exp. 13	9				
	Exp. 47	10				
	Exp. 38	11				
3	Exp. 19	7	0.05	3	85	PO_4^{-3} added to Ca^{2+}
	Exp. 16	9				
	Exp. 36	11				

RAO: reactants addition order, RA: reactants addition rates.

Table 4. Experiment sets ran to study the effect of reactant addition rate

Set no.	Exp. no.	RA mL/min	$[Ca^{2+}]$ mol/L	pH	T (°C)	RAO
1	Exp. 28	0.8	0.01	9	25	PO_4^{-3} added to Ca^{2+}
	Exp. 39	1.3				
	Exp. 7	3				
	Exp. 55	4				
2	Exp. 29	0.8	0.01	9	85	PO_4^{-3} added to Ca^{2+}
	Exp. 33	1.3				
	Exp. 10	3				
	Exp. 56	4				

RAO: reactants addition order, RA: reactants addition rates.

the structural characteristics of the powder and SEM was used to characterize the morphology of the powder. The quantitative analysis was carried out by the Rietveld refinement method, which was used in combination with the XRD patterns. The EDX was used to monitor the Ca/P ratio.

Qualitative X-ray diffraction (XRD) was done in micro diffraction mode with CuKα radiation ($\lambda = 1.5418$Å) on a DISCOVER D8 diffractometer (Bruker, Germany) with θ/θ geometry, 0.5 mm beam size and General Area Diffraction Detector System (GADDS). The XRD data were collected at 40 kV and 40 mA. Samples were positioned using a xyz sample stage with video microscope. Frames of data were collected for 1 min each, integrated and merged to produce a diffraction pattern from 10–100° 2θ with step size of 0.04°. The FTIR analyses were performed using Bruker IFS 55 FTIR spectrometer. All samples were ground and mixed with KBr, and then placed on a sample holder and pressed at a high pressure to form pellets. The samples analyzed on the EDX and SEM, were sputtered–coated with gold before being analyzed. The SEM images and the EDX were performed using Hitachi S4500 field emission scanning electron microscopy and EDAXT Phoenix model with light element detection. The volume-weighted mean particle size was measured using a Malvern Matersizer that uses the Mie theory for measuring and data analysis. All the samples were measured in a wet condition. A suspension medium was prepared by filtering the mother liquid from the corresponding experiments to ensure saturation with respect to hydroxyapatite.

Quantitative XRD analysis was done on a Rigaku Bragg Brentano geometry from 10–90° 2θ with a step size of 0.05°. DIFFRAC^{plus} EVA 7.0 software was employed in data analysis. The crystalline phase was identified from a comparison of the registered patterns with the ICDD (International Center for Diffraction Data) powder diffraction file (PDF, pattern 72–1240). DBWS program (24) was used to refine some of the

samples using Rietveld refinement procedures. All samples were ground to a fine powder for 30 min and then mounted in the sample holder.

RESULTS AND DISCUSSIONS

Morphology and Crystallinity

The SEM Results

The SEM images revealed the effect of different synthesis parameters on the particles morphology and crystallinity. The effects of each parameter as revealed by the SEM are discussed below:

The Temperature Effect

Figure 3 shows the effect of synthesis temperature on the morphology and crystallinity of the powder. Samples Exp. 50, Exp. 51, Exp. 16, Exp. 54 were all synthesized at pH = 9, initial calcium concentration 0.05 M and reactant addition rate 3 L/min. Figures 4 and 5 show the effect of temperature, but at different synthesis conditions. See Table 1 for the synthesis conditions. Figures 3–6 show that the temperature has a pronounced effect on the crystallinity of the particles. The higher the synthesis temperature, the higher the crystallinity of the powder is. Samples synthesized at 44 and 60°C showed a very similar morphology. They are irregular small plate-like crystals. Small agglomerates were observed as well. For the samples synthesized at 55°C, the crystals are rod-like and they are larger compared to those synthesized at 44, 60, and 85°C. The crystals produced at 85°C had flake-plate-like crystals. Small agglomerates were observed in this sample. Figure 4 shows two other samples from Exp. 19 and Exp. 37. Both were synthesized at the same conditions but at different temperatures, 25 and 85°C respectively. The one synthesized at 25°C is more agglomerated and it has low crystallinity. On the other hand the one synthesized at 85°C is more crystalline and the crystals have more defined edges with plate-like shape. The same effect of temperature was observed in Exp. 23 and Exp. 24 as shown in Figure 5. One can realize the obvious enhancement in crystallinity as the temperature increases to 85°C. Sample Exp. 23 is most likely amorphous while Exp. 24 is almost totally crystalline with plate-like shape.

The pH Effect

The effect of synthesis pH is shown in Figs. 6 and 7. Figure 6 shows powder images synthesized at an initial calcium ion concentration of 0.01 M. Exp. 10 and Exp. 44 synthesized at pH 9 and 8, respectively, show very similar morphological shape. The crystals are plate-like. They only differ in the size, where crystals synthesized at pH 9 are somewhat larger than those synthesized at pH 8. Samples synthesized at pH 11 (Exp. 31)

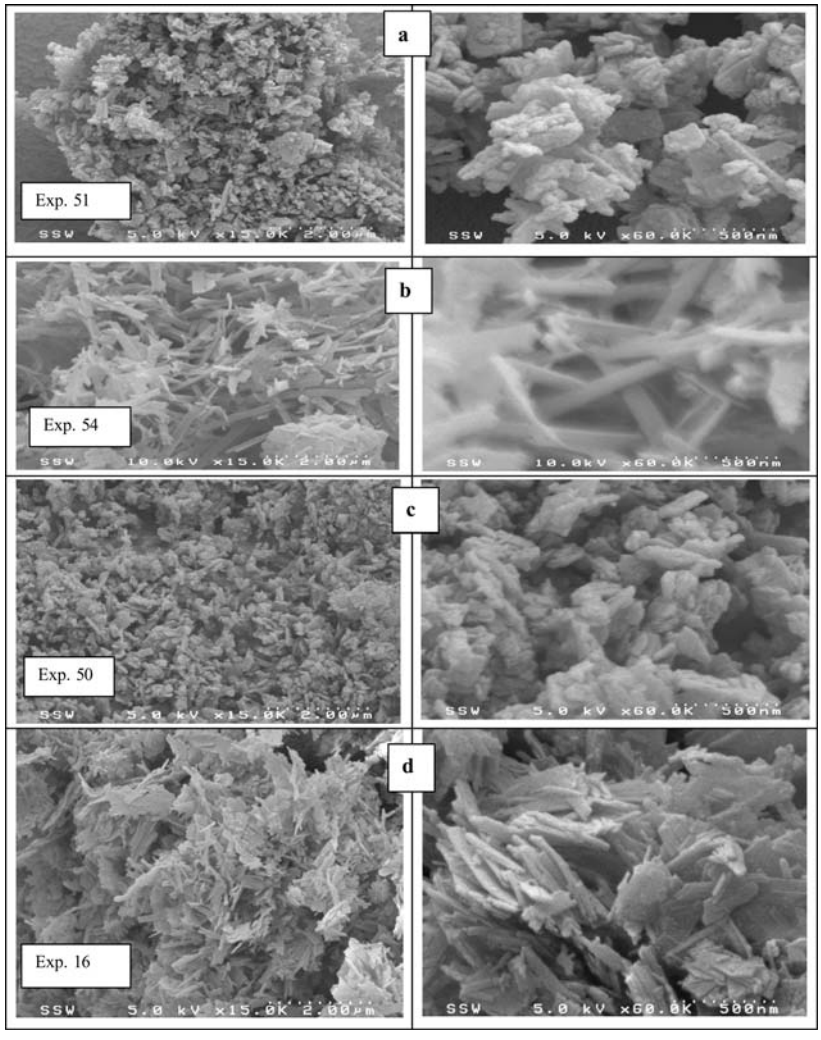

Figure 3. SEM images for samples synthesized at $[Ca^{2+}] = 0.05\,M$, pH = 9, and addition rate of 3 L/min, and aging time of 8 hours a) $T = 44^{\circ}C$, b) $T = 55^{\circ}C$, c) $T = 60^{\circ}C$, and d) $T = 85^{\circ}C$.

show a very different morphology, where the crystals are smaller with flake-like shapes. They also exhibit more agglomeration. The sample synthesized at pH 10 (Exp. 46) shows crystals with very defined edges and rod-like shape. The crystal size is the largest in Exp. 46 among all. The effect of pH at higher concentration (calcium concentration of 0.05 M) is shown in Figure 7. The three powders show almost the same morphology, no big difference is observed among the three powders. They are irregular plate-like

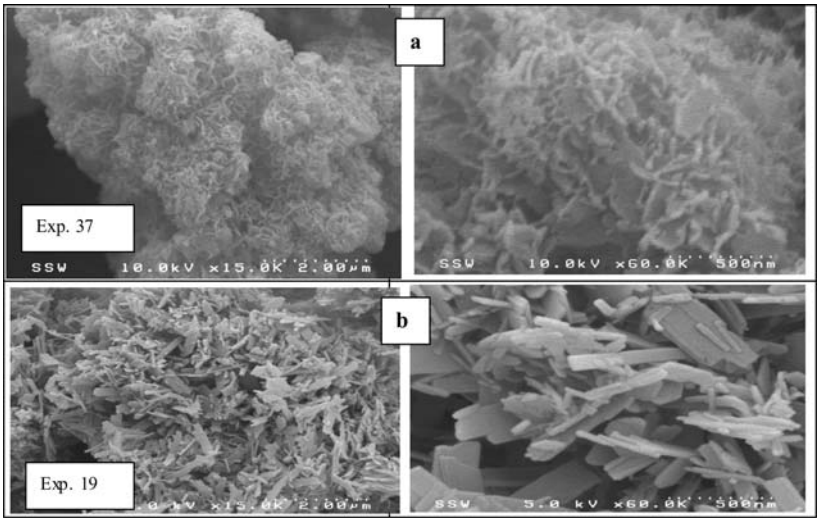

Figure 4. SEM images for samples synthesized $[Ca^{2+}] = 0.05\,M$ and $pH = 7.4$, reactant addition rate $3\,mL/min$, and aging time of 8 hours a) $T = 25^{\circ}C$, and b) $T = 85^{\circ}C$.

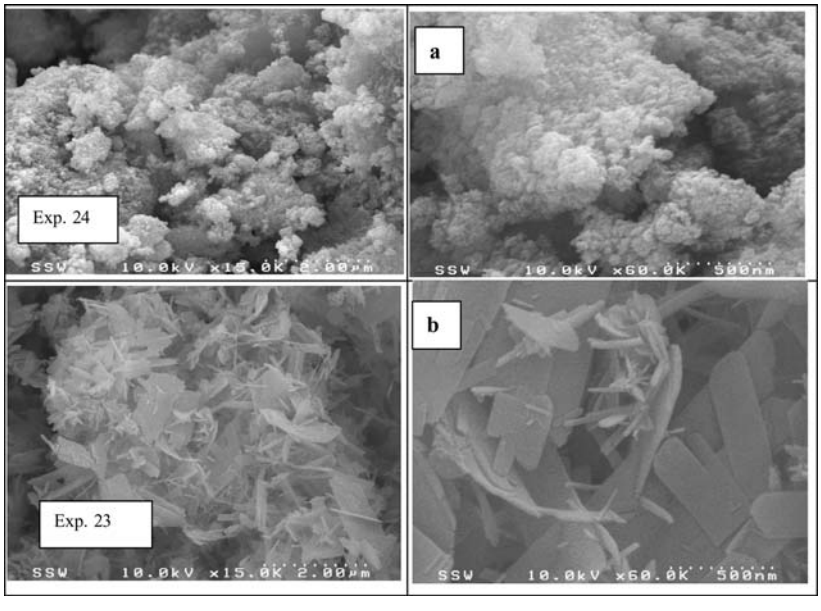

Figure 5. SEM images for samples synthesized $[Ca^{2+}] = 0.01\,M$ and $pH = 9$, reactant addition rate $3\,mL/min$, and aging time of 4 hours a) $T = 25^{\circ}C$, and b) $T = 85^{\circ}C$.

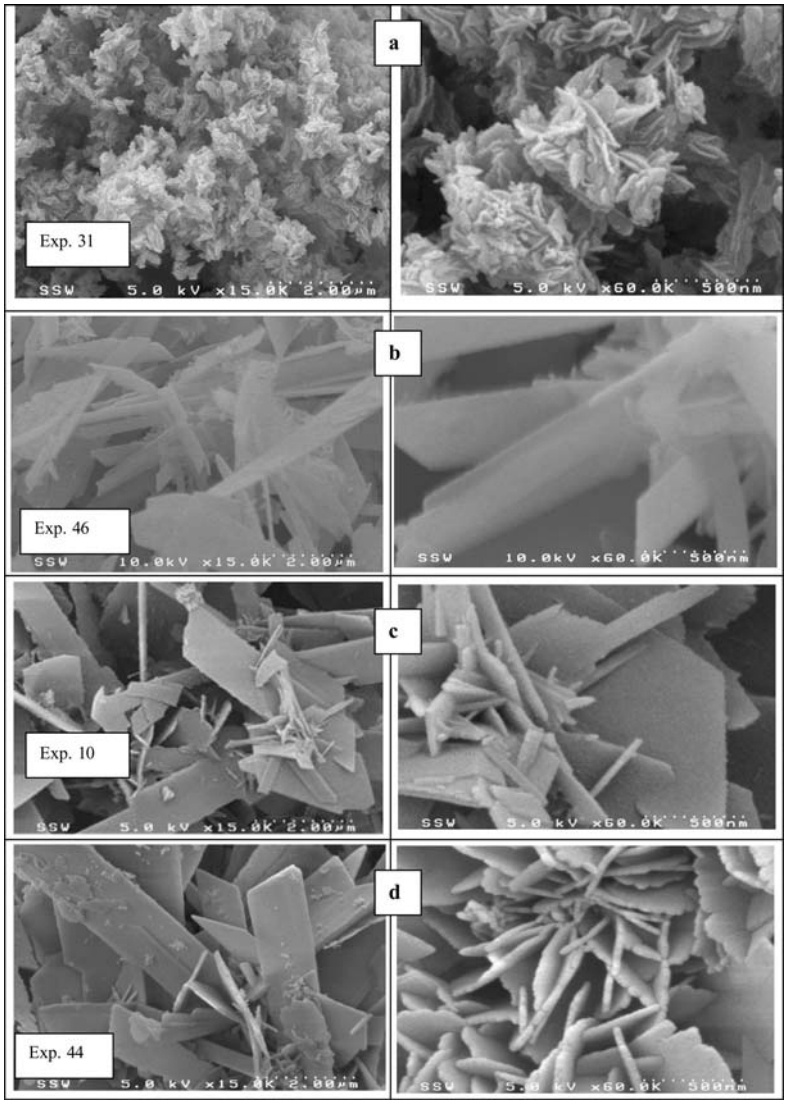

Figure 6. SEM images for samples synthesized $[Ca^{2+}] = 0.01\,M$ and $T = 85^{\circ}C$, reactant addition rate 3 mL/min, and aging time of 8 hours a) pH = 11, b) pH = 10, c) pH = 9, d) pH = 8.

crystals. The effect of initial concentration is ascertained by comparing the morphology of the crystals in Figure 7 with those in Figure 6. Lower concentrations give more uniform crystal shapes and larger crystals, while at higher initial concentrations particles tend to form agglomerates. The effect of changing the pH on the morphology at lower concentration is more obvious

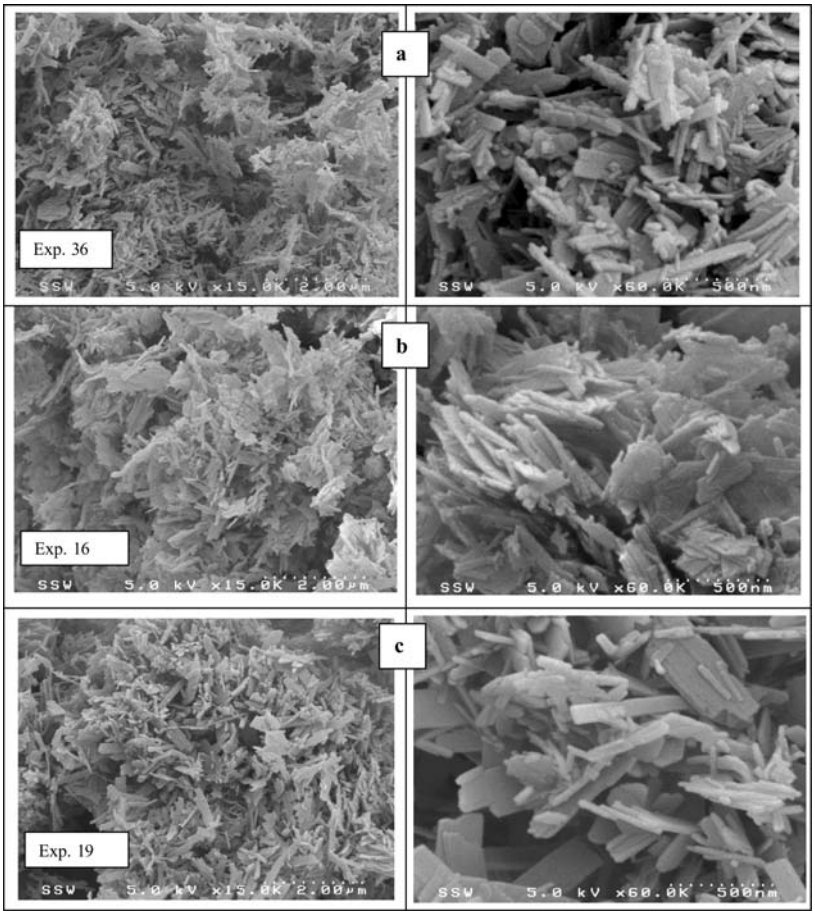

Figure 7. SEM images for samples synthesized at $[Ca^{2+}] = 0.05\,M$ and $T = 85^{\circ}C$, reactant addition rate 3 mL/min, and aging time of 8 hours a) pH = 11, b) pH = 9, c) pH = 7.4.

than those synthesized at higher concentrations. The pH almost has no effect at higher concentrations.

The Effect of the Reactant Addition Rate

The reactant addition rate was varied from 0.8–4 mL/min. Several experiments as shown in Table 1 were conducted at various reactant addition rates. Figures 8 and 9 show the effect of changing the reactant addition rate on the overall morphology of crystals synthesized at 25 and 85°C. Figure 8 shows the morphology of the powders synthesized at 85°C but and reactant addition rates of 0.8, 1.3, 3 and 4 mL/min. Samples synthesized at addition rates of 1.3 and 0.8 ml/min (Exp. 33 and Exp. 29) show

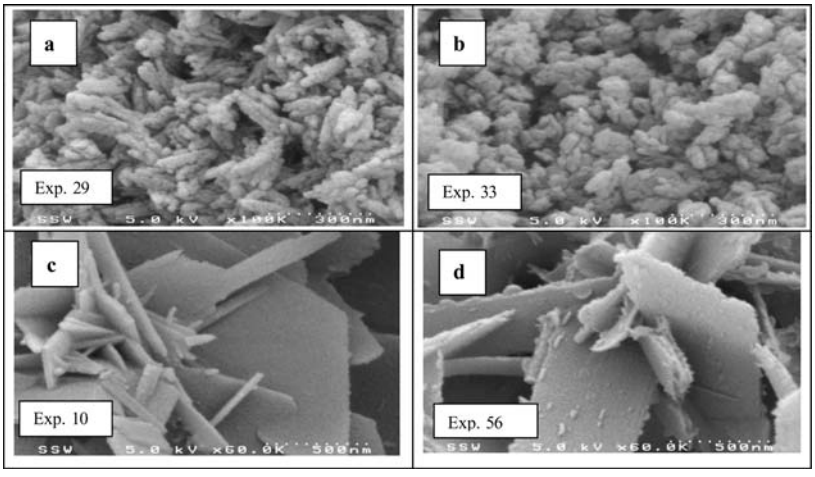

Figure 8. SEM images for samples synthesized at $[Ca^{2+}] = 0.01$ M and T = 85°C, aging time of 8 hours, pH = 9, and reactant addition time of a) 0.8 mL/min, b) 1.3 mL/min, c) 3 mL/min, and d) 4 mL/min.

very similar morphology, where both formed very small agglomerates. The SEM images of these two samples were taken at higher magnification to see the small agglomerates. The particles appeared to be in between amorphous and crystalline phase and with rod like shapes. Samples synthesized at a rate of 3 mL/min (Exp. 10) showed larger crystals, well-defined crystal edges and smooth crystal surface. Samples synthesized at a rate of 4 mL/min (Exp. 56) showed crystals similar to Exp. 10 but with smaller particles attaching to the surface of the crystal plates with no distinct edges. Crystals of Exp. 10 are smaller in size compared to those produced at faster reactant addition rates. For samples synthesized at the lower temperature (25°C), the reactant addition rate affected the crystallinity. Samples synthesized at lower reactant addition rate (Exp. 39) showed better crystallinity. The crystal shape is more defined, although agglomeration is still present. The other two samples (Exp. 9 and Exp. 55) exhibit no order or crystallinity.

The FTIR Results

The FTIR analyses were done for few samples to detect the presence of the characteristic peaks of HAP. All samples showed the characteristic peaks of HAP, which are PO_4^{-3}, OH^{-1} groups.

The Temperature Effect

Experiment Exp. 19 synthesized at 85°C and the conditions shown in Table 1 exhibits high intensity peaks at 1032, 962, 875, 604, 563 cm^{-1} that correspond to PO_4^{-3} group. Small intensity peaks were located at 3420 and

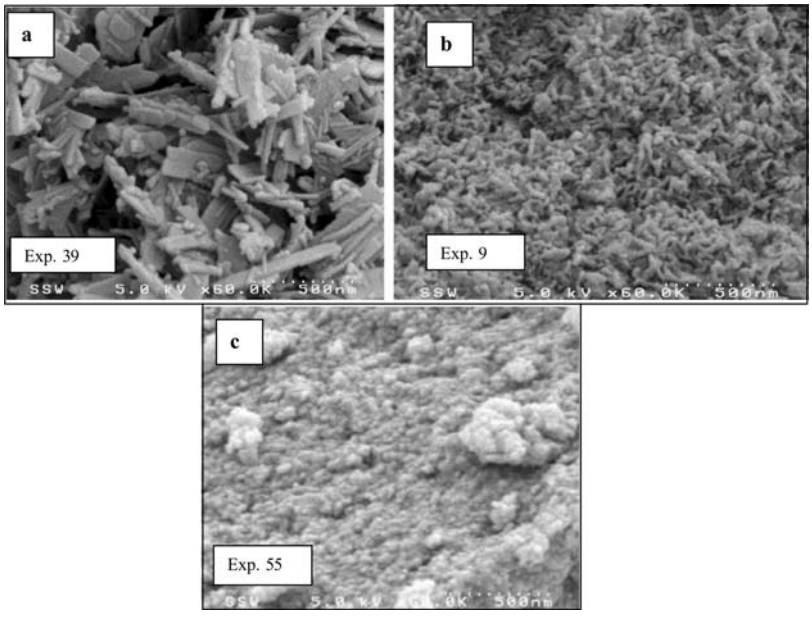

Figure 9. SEM images for samples $[Ca^{2+}] = 0.01$ M and T = 25°C, pH = 9, aging time of 8 hours, and reactant addition time of a) 1.3 mL/min, b) 3 mL/min, c) 4 mL/min.

1641 cm^{-1} that correspond to H_2O. Another small intensity peak was found at 3571 cm^{-1}, which was attributed to OH^{-1} group. Two very tiny intensities were found at 1458 and 1422 cm^{-1} that showed the presence of some carbonates with very low concentrations. Looking at the FTIR results obtained from Exp. 37, which was synthesized exactly at the same conditions of Exp. 19 but at lower temperature (25°C), the PO_4^{-3} peaks at 1034, 960, 603, and 564 cm^{-1} are still present but with much lower intensities. The carbonate concentrations were also located at 1464 cm^{-1}. A broad absorption band of OH^{-1} was found at 3399 cm^{-1}. The broadening of OH^{-1} peak and the lower intensities of PO_4^{-3} group revealed the lower crystallinity of this sample compared to Exp. 19, which is in agreement with the SEM images. Also the OH^{-1} peaks were not present in this sample, only a very small peak of OH^{-1} was found at 1641 cm^{-1} (see Figure 10). Usually broader peaks of H–O–H and H–O bands indicate that O–H bond is present at different sites (25). Therefore the identified OH^{-1} could belong to HAP molecule, water molecule, or other calcium phases, such as amorphous. The peak located at around 875 cm^{-1} was detected in both samples. This peak could be attributed to either carbonates or PO_4^{-3} groups. No peaks were detected at 1208 or 868 cm^{-1}, which correspond to HPO_4^{-2} group (6). The absence of this group indicates that there is no other calcium phosphate phases present.

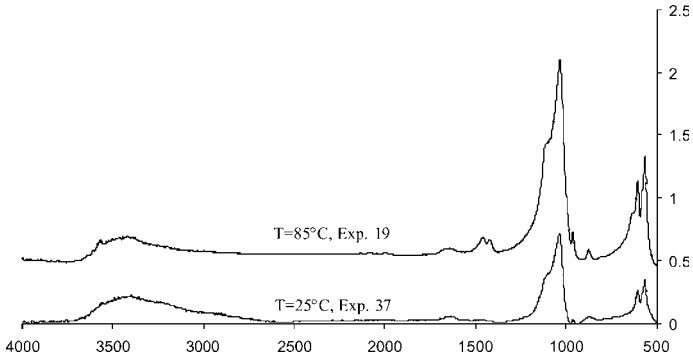

Figure 10. FTIR of EXP37 and EXP19 synthesized at pH = 7.4, $[Ca^{2+}] = 0.05\,M$, $3\,mL/min$, and the above two temperatures.

The effect of synthesis temperature was also studied using the FTIR results of samples Exp. 16, Exp. 50, Exp. 54, and Exp. 51 in Fig. 11. These samples were synthesized at 85, 60, 55, and 44°C, respectively. The increase in the PO_4^{-3} intensity with temperatureis very clear. Also the H_2O peaks became broader and less intense as the temperature decreased. The peak at $3572\,cm^{-1}$ corresponds to OH^{-1} group and was only observed in Exp. 16. Very few differences were observed between sample Exp. 51 and Exp. 54. Sample Exp. 51 has stronger H–O peak compared to Exp. 54. The carbonate groups were detected in all samples and they almost have the same carbonate concentration.

The pH Effect

The effect of pH was not very noticeable as the temperature effect. The FTIR results of Exp. 19, Exp. 16, and Exp. 36 synthesized at 0.05 M of

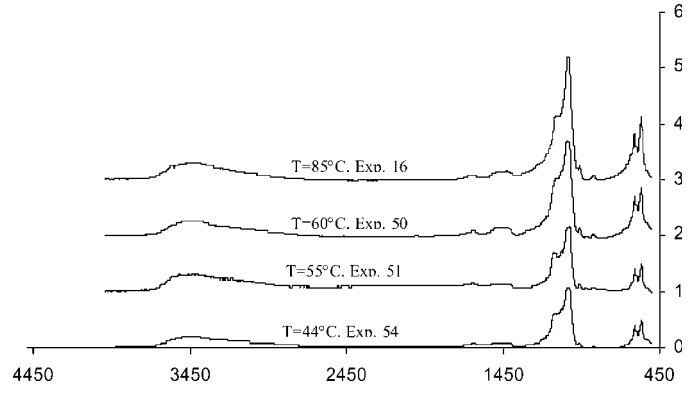

Figure 11. FTIR of samples synthesized at pH = 9, $[Ca^{2+}] = 0.05\,M$, and reactant addition rate of $3\,mL/min$, and at the above indicated temperatures.

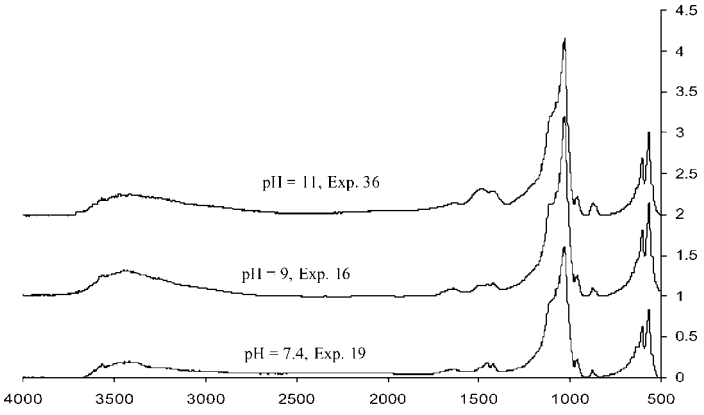

Figure 12. FTIR of samples synthesized at T = 85°C, $[Ca^{2+}] = 0.05$ M, reactant addition rate 3 mL/min and the above shown pH.

calcium ions and pH 7, 9, and 11 are shown in Fig. 12. The characteristic peaks of HAP are present in all the samples, with slightly higher intensity of PO_4^{-3} group in samples Exp. 16 and Exp. 36. Exp. 19 showed narrower H_2O and OH^{-1} peaks compared to the other two samples. Overall the three samples indicated the presence of high crystalline HAP. The SEM images are in agreement with the FTIR results, where it showed plate-like crystals. At lower calcium ion concentration (0.01 M) Exp. 44, Exp. 10, Exp. 46 and Exp. 31 were synthesized at pH 8, 9, 10 and 11, respectively. The PO_4^{-3} intensities were lower than those synthesized at higher calcium ion concentration. This is expected since the peaks intensity depends also on the concentration of the material. Experiment 46 and Exp. 10 had higher PO_4^{-3} intensities compared to Exp. 44 and Exp. 31, which indicated higher crytsatllinity. This points out that synthesizing HAP at pH 9 and 10 gives better crystallinity. High concentration of carbonates was found in Exp. 46 and Exp. 31. Stronger but broader H–O peaks were found in Exp. 46 and Exp. 31. This broadening could be attributed either to the presence of absorbed water or the incorporation of carbonates in the lattice of the crystal. The second reason is more probable since these two samples contained slightly higher carbonate concentrations. However samples synthesized at lower pH (9 and 8) in Exp. 10 and Exp. 44 showed weaker and less intense peaks of H–O bonds with a lower intensity in sample Exp. 44. New peaks were detected in Exp. 10 at 803, 1262 and 2964 cm^{-1}. These peaks were identified as silicon. The presence of silicon is attributed to the use of silicon oil in the heating jacket of the reactor, which must have contaminated this sample.

The Effect of the Reactant Addition Rate

At synthesis temperature 85°C, addition rates of 0.8, 1.3, 3 and 4 mL/min were used in experiments Exp. 29, Exp. 33, Exp. 10 and Exp. 56. Results are

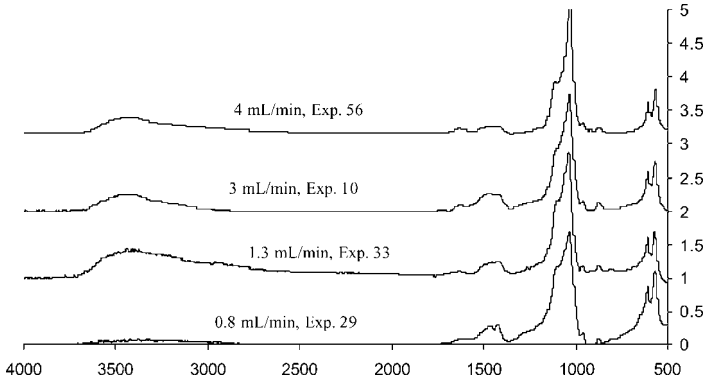

Figure 13. FTIR bands of samples synthesized at T = 85°C, $[Ca^{2+}] = 0.01\,M$, pH = 9, and the above reactant addition rate.

shown in Fig. 13. Exp. 56 showed the highest PO_4^{-3} peaks intensity compared to others and a strong OH^{-1} absorption band at $3246\,cm^{-1}$, in addition to another O–H peak at $1639\,cm^{-1}$. The peaks appeared sharp and very similar to the standard HAP peaks of the FTIR bands. The other three samples were almost similar, only Exp. 29 has higher carbonates bands at 1423 and $1461\,cm^{-1}$. Also a small peak at $1265\,cm^{-1}$ was observed here. This peak was attributed to some silicon contamination from the silicon oil used in the reactor. Another peak is detected in this sample at $1580\,cm^{-1}$. Carbonate groups were observed in all samples. The presence of stronger peaks of H–O in Exp. 56 revealed the higher crystallinity of this sample compared to the other samples. SEM images revealed high crystallinity of this sample as well. Exp. 29 showed the weakest H–O band, which indicates the low crystallinity of this sample compared to the others. This showed that higher reactant addition rate at this temperature produces more crystalline powder. It is important to mention that the intensities of the FTIR absorption bands are not always a good indication of the crystallinity of the sample. Other factors could affect the intensity of the bands such as the concentration and the amount of material analyzed. At lower synthesis temperature (25°C), Exp. 55, Exp. 9 and Exp. 39 were synthesized at addition rate of 4, 3 and 1.3 mL/min, respectively. Broader PO_4^{-3} peaksare present in Exp. 9 and Exp. 55. The highest intensity peaks were observed in Exp. 55. The SEM images of Exp. 55 did not show any ordered structure; therefore the higher intensity peaks in this sample might be attributed to other factors such as the amount of the sample analyzed and not to the crystallinity of the sample.

During the run Exp. 14, two samples were taken. The first one was taken after 2 hours, and the second one after 4 hours. The FTIR of those samples (Fig. 14) were preformed and showed clearly the transformation to HAP after a period of time. The first sample S_1 showed the presence of extra peaks at 1221.04, 1133, 788.93, 655.64, 524.9, 3165.43 and $3271.98\,cm^{-1}$. Those peaks

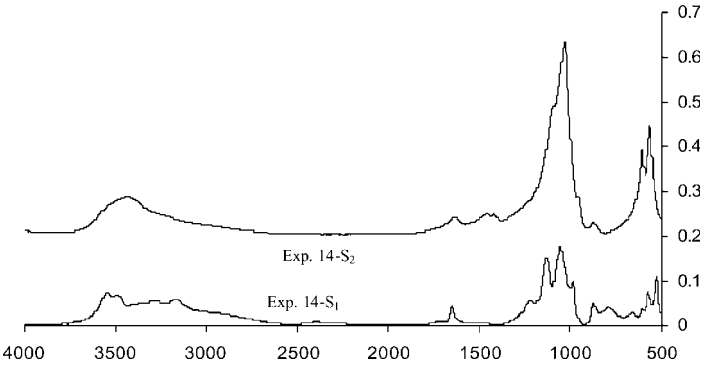

Figure 14. FTIR bands of EXP14 for two samples S_1 and S_2 taken after 2 hours and 4 hours, respectively.

disappeared completely after 4 hours, as can been seen in S_2. The FTIR results of S_2 showed the typical HAP characteristic peaks, but the intensity of the PO_4^{-3} group is low and broad. Carbonate bands at 1457.39 and 1422.75 cm^{-1} appeared in this sample. In experiment EXP10, three samples were taken during the precipitation process, after 2 hours, after 4 hours and after 8 hours. All three samples showed the typical HAP characteristic peaks. This confirmed that the conversion to HAP at higher temperature is much faster.

The EDX Results

The energy dispersive X-ray spectrometry (EDX) was performed to determine the Ca/P ratio in the final product. Two spots in each sample were analyzed to study the homogeneity of the samples. Table 5 shows that the Ca/P ratio of all the samples was in the range between 1.4–1.9. Most of the samples showed non-homogeneity in the compositions from spot to spot, such as Exp. 55, Exp. 19, and Exp. 33. This revealed that using the Ca/P ratio as an indication of the presence of HAP cannot always be trusted and the calcium and phosphors concentrations measured could be an average value. Besides, other calcium phosphate compounds could be present and affect this average value. In general all the samples showed a Ca/P ratio very close to the stiochiometric ratio of HAP, which is 1.67. The EDX analysis revealed the presence of silicon in some of the samples, with a very high concentration in sample Exp. 32. It appeared that silicon incorporation occurred as a result of evaporation of the heating oil and its absorption in the liquid inside the reactor.

The XRD Results

The X-ray diffraction pattern of all samples showed an HAP profile, with some variation in crysallinity. Figure 15 shows the XRD patterns of Exp. 26,

Table 5. The Ca/P ratio of different samples as obtained using the EDX

Sample name	Spot one	Spot two
Exp. 16	1.57	1.63
Exp. 39	1.46	1.57
Exp. 51	1.40	1.36
Exp. 29	1.57	1.73
Exp. 31	1.60	1.56
Exp. 33	1.48	1.89
Exp. 27	1.64	1.54
Exp. 7	1.42	1.46
Exp. 50	1.46	1.38
Exp. 44	1.55	1.55
Exp. 36	1.50	1.49
Exp. 54	1.46	1.4
Exp. 56	1.46	1.47
Exp. 46	1.60	1.70
Exp. 53	1.70	1.63
Exp. 32	1.57	1.53
Exp. 19	1.50	1.60
Exp. 55	1.64	1.45
Exp. 10	1.45	1.59

Exp. 25, and Exp. 27. The samples as indicated in Table 1 were synthesized at room temperature with calcium ion concentration 0.007 M and at pH = 9. The only difference is the reactant addition order as indicated in Table 1. A standard HAP pattern was included for comparison. As it is clear the main peaks of HAP were present in all three samples. The three samples did not show any significant differences, they were almost identical.

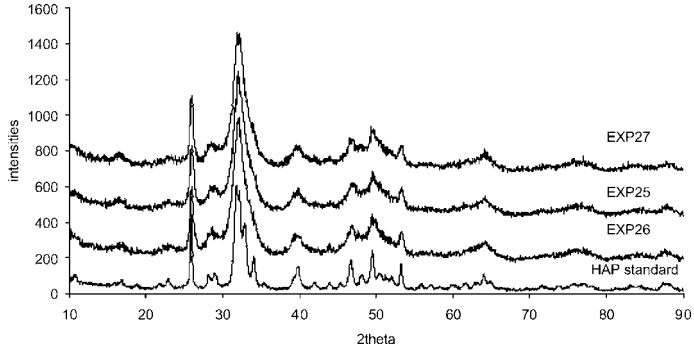

Figure 15. The XRD patterns of samples synthesized at T = 25°C, pH = 9, calcium ion concentration 0.007 M, and at different reactant addition order see Table 1.

This indicated that the reactant addition order did not have a noticeable effect on the quality of the final product. The peaks of these three samples were much broader compared to the standard HAP indicating the lower crystallinity.

Figures 16 and 17 show the XRD pattern of Exp. 19 and Exp. 37. The effect of temperature on the crystallinity is very clear. Higher temperatures resulted in sharper intensities and narrower peaks suggesting more crystallinity.

There was no significant effect of pH changes on the final powder. Figure 18 shows two XRD patterns synthesized at 0.05 M calcium ion concentrations with pH 9 at pH 11 (Exp. 16 and Exp. 36).

The Mean Particle Size

The effects of temperature, pH and reactant addition rate on the mean particle size were studied.

The Temperature Effect

The effect of temperature over the range from 25 to 85°C, on the mean particles size is shown in Figure 19. The mean particle size shows a minimum at a temperature between 45 to 55°C. The mean particles size at room temperature in all experiments was in the range of 27 to 40 μm. As the temperature increased to 44°C, a drop in the mean particle size from 5 to 20 μm, was noticed. As the temperature increased more the particle size increased again. Liu et al. (12) reported that the mean particle size increased as the temperature decreased from 60°C to 15°C. Riman et al. (27) showed that the mean particle size at 200°C was larger than at 55°C. As the temperature increases from 25°C to 44°C, the reaction or conversion rate increases producing higher supersaturation in the solution, which

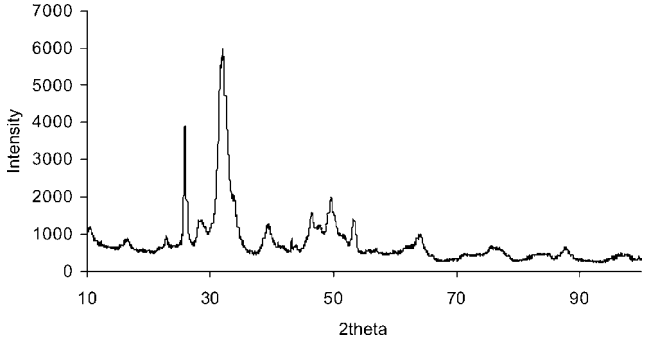

Figure 16. XRD pattern of sample EXP37 synthesized at 25°C, pH = 7.4, $[Ca^{2+}] = 0.05$ M, and reactant addition rate 3 mL/min.

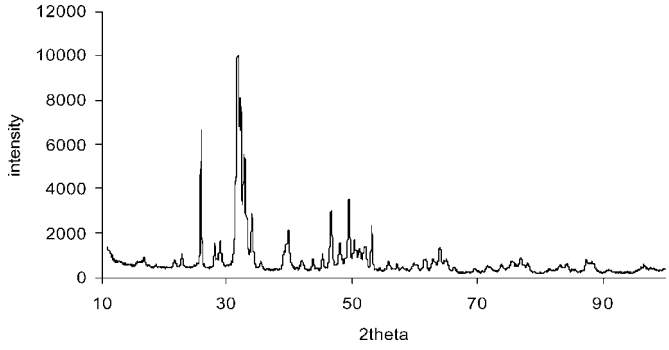

Figure 17. XRD pattern of sample EXP19 synthesized at 85°C, pH = 7.4, $[Ca^{2+}] = 0.05$ M, and reactant addition rate 3 mL/min.

promotes nucleation leading to a smaller mean particle size. Above the temperature range of 44°C to 55°C, higher supersaturation produces very tiny crystals. However, the agglomeration rate also increases leading to larger mean particle size (28). The agglomeration of the particles was confirmed by SEM photographs.

The pH Effect

The effect of pH on the mean particle size is shown in Figure 20. The relationship is non-linear and shows a maximum at pH 9. This implies that the growth rate is favored at a pH around 9 and it decreases above and below this pH. At pH 11 the particle size shows an increase for the set of experiments synthesized at 25°C and 0.05 M calcium ion concentrations. The increase in

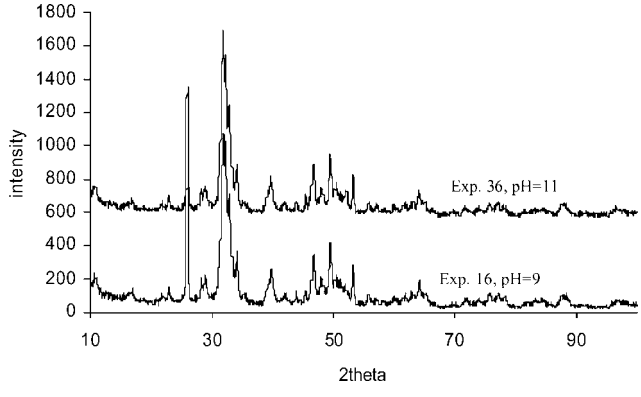

Figure 18. XRD pattern of sample EXP16 and EXP36 synthesized at 85°C, $[Ca^{2+}] = 0.05$ M, reactant addition rate 3 mL/mint and at the above pH values.

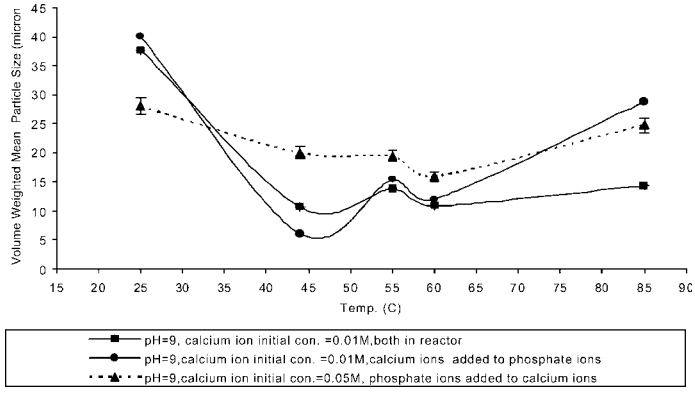

Figure 19. The dependence of the mean particle size on temperature.

the growth rate at around pH 9–10 suggests a lower supersaturation. The pH changes affect the concentration of the reacting ions, which in turn has a large effect on the degree of supersaturation. A study conducted by Boskey and Posne (5) showed that the induction period that was observed at the beginning of the reaction in calcium phosphate systems is a function of the pH of the system. This induction period was found to increase as the pH increased. This means that the conversion or the reaction rate is slower at higher pH values, which in turn lowers supersaturation. They worked in the pH range from 6.8 to 10. They observed an increase in the mean particle size at pH 9–10. A study conducted by Meyer and Eanes (6) showed similar results. They conducted experiments at the pH values from 7.4 to 9.25. The amorphous calcium phosphate solubility was found to decrease

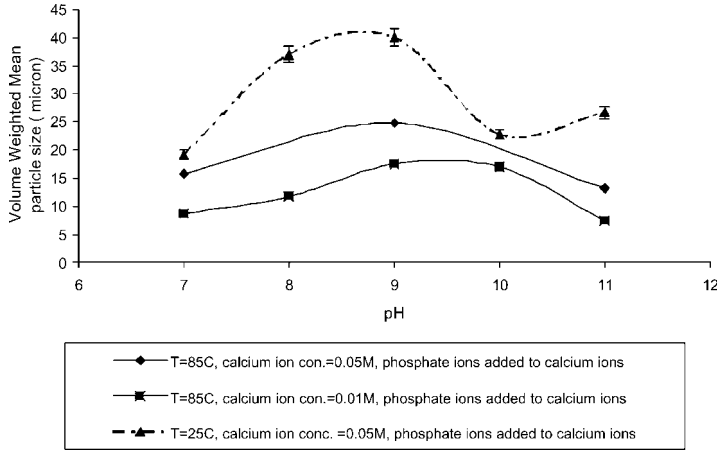

Figure 20. The dependence of the mean particles size on the pH.

with increasing pH, which means the conversion from amorphous to crystalline HAP is slower at higher pH values. Neither studies (5, 6) covered pH 11, as presented in the present work. We observed an increase in the conversion rate and the reaction rate at this pH value that produced higher supersaturation in the system.

The effect of initial reactant concentration on the mean particle was also studied. The third set of experiments at 85°C and calcium ion concentration equal to 0.05 M showed slightly larger mean particle size compared to set one (85°C and 0.01 M calcium ion concentration). This increase in the mean particle size might be a result of the agglomeration in these samples as it had been indicated in the SEM images.

The Effect of the Reactant Addition Rate

Figure 21 shows the changes in the mean particle size with increasing reactant addition rate. Two sets of experiments were performed, one at 25°C and the other one at 85°C. Both showed the same behavior. At a very slow rate of addition, the mean particle size was larger and then decreased at a flow rate of 1.3 mL/min. Further increase in the reactant addition rate, increased the mean particle size as shown in Fig. 21. At low addition rates, a more homogeneous distribution of supersaturation is achieved, which results in an increase of the growth rate. At high addition rates, the growth rate is again favored over the nucleation rate, which leads to an increase in the mean size. The reactants are introduced through an inlet tube. Blobs of reactants are formed due to the surface tension. At high reactant addition rates the blobs of the reactants are large and reach the impeller where they break up and form smaller blobs that spread all over the reactor. When the big blobs

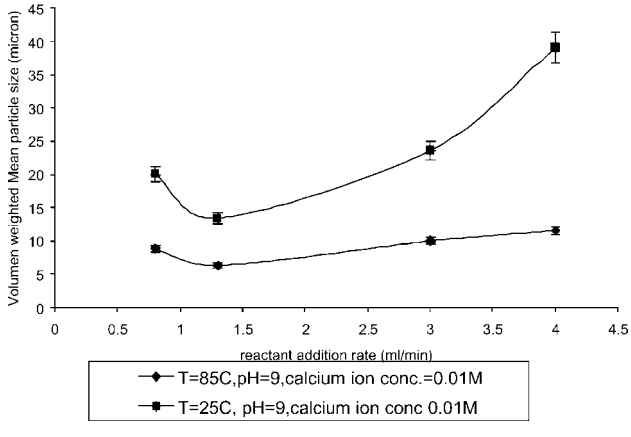

Figure 21. The dependence of the mean particles size on the reactant addition rates.

split to smaller blobs, the interfacial surface area between the reactants increases and produces lower supersaturation that favors growth rate over nucleation rate. For the intermediate addition rates, are not large enough to break extensively and the surface area between the reactants is smaller, therefore nucleation is favored.

Determination of the Purity of the HAP

In order to determine the purity of the resulting HAP, a precise quantitative analysis method is required. Chemical elemental analysis determines the sodium, calcium, and phosphorus content of the synthesized powder. It does not, however, determine the actual phase composition of the resulting calcium phosphates. Indeed, obtaining a Ca/P ratio close to 1.67, does not guarantee the presence of pure hydroxyapatite. Other calcium phosphate phases have lower and higher Ca/P ratios that may average out to 1.67. The only reliable analytical technique that can render quantitative results on phase composition is X-ray diffraction coupled with the Rietveld algorithm. Therefore, the Rietveld refinement method with the XRD results were used in the present study for the quantitative analysis of the synthesized powder. The prospective reader is referred to Al-Qasas (26) for the details of the quantitative analysis technique. A software program (DBWS) was used to refine the crystal structure of HAP with and without extra phases. Samples from three experiments (Exp. 33, Exp. 19, and Exp. 50) were examined. The detailed description of the refinement procedure is presented elsewhere (26). The results revealed that samples synthesized at 85°C were pure HAP with good crystallinity. No other phases were present. The OCP and TTCP phases were considered as other phases that might be present but the refinement indicated that none of these phases were present. Exp. 33 showed the best refinement results, where the fitting criteria ($R_{wp} = 9.71$ and $R_B = 4.5$) dropped below the required tolerance limits. Exp. 19 showed a good fit as well, but the R_{wp} and R_B did not go below the required values, but they were very close. Also no other phase was identified in this sample. Exp. 50 showed the presence of OCP phase besides the HAP phase. Unfortunately for Exp. 50 the refinement could not proceed to completion and the exact percentage of OCP was not obtained. This was due to the inaccurate OCP crystal structure found from literature (29).

CONCLUSIONS

A highly crystalline HAP powder was synthesized at selected operating conditions. The temperature played the most important role in the enhancement of the crystallinity. Samples produced at 85°C showed the highest

degree of crystallinity. The transformation from amorphous to crystalline HAP was faster at higher temperatures and this is in agreement with all previous authors. This is due to the decrease of HAP solubility at higher temperatures and the addition of energy, which accelerates the HAP nuclei formation. The pH in the range 7–11 showed to affect the morphology and the crystal size more than the crystallinity of the powder. Also the effect of pH on the morphology was more pronounced at lower concentration of the reactants. Powders produced at low reactants concentrations and pH 11 showed different morphology. Many authors have previously reported the effect of pH (9, 10, 17). Seckler et al. (9), and Rodriguez-Lorenzo and Vallet-Regi (10) agreed that higher pH produces higher crystalline powders, while Kim et al. (17) reported the opposite. Optimum crystallinity can be obtained over a certain range of pH values. The effect of the reactant addition rate differs at different temperatures. At 85°C, faster reactant addition rate produced larger crystals with less agglomeration and high crystallinity. While at slower addition rate, smaller particles appeared with rod-like shapes and lots of agglomerations. At lower temperature (25°C), and slower reactant addition rate, well-defined crystals were obtained, while samples synthesized at higher addition rate did not show any evidence of the presence of any ordered structure. This actually agrees with the findings of Seckler et al. (9). In some samples carbonates were formed, which suggested the incorporation of the carbonate groups in the lattice, and possible formation of carbonated apatite. The refinement results showed that the powder produced in Exp. 33 was almost pure HAP. This indicates that slower addition rate higher temperature and lower initial reagent concentrations are the most dominant factors in the production of pure HAP. At a temperature lower than 85°C other calcium phosphate phases form beside the HAP. The reactant addition order has no effect on either the crystallinity or the structure of the powder, which contradicts what Torrent-Burgues and Rodriguez-Clemente (13) have reported.

The mean particle size showed a large dependency on pH, temperature and reactant addition rate. Higher temperatures favor the nucleation rate. At high temperatures (85°C) particles tend to form agglomerates that increase the observed mean particle size. The mean particle size showed a peak at pH 9. It appeared that at that pH the reaction rate and the supersaturation are minimum, therefore the growth rate is favored in comparison to the nucleation rate and leads to the formation of a large mean particle size. The mean particle size increased with the increase of the reactant addition rate for both temperatures 25 and 85°C. At very slow addition rate (0.8 mL/min), the mean particle size was slightly larger compared with an addition rate of 1.3 mL/min. A more detailed kinetic study of the nucleation and growth kinetics of calcium phosphate systems and the mechanism of formation of HAP are still required.

ACKNOWLEDGMENT

We would like to thank the University of Western Ontario and the Natural Sciences and Engineering Research Council of Canada for the financial support of this project.

REFERENCES

1. Amjad, Z. (1998) *Calcium Phosphates in Biological and Industrial Systems*; Kluwer Academic Publishers: Boston.
2. Elliott, J.C. (1994) Structure and Chemistry of the Apatities and Other Calcium Orthophosphates. In *Studies in Inorganic Chemistry*; Amsterdam: New York: Elsevier.
3. Sudarsanan, K. and Young, R.A. (1969) Significant precision in crystal structural details: Holly Springs hydroxyapatite. *Acta Crystallog.*, B25: 1534–1543.
4. Eanes, E.D., Gillessen, I.H., and Posner, A.S. (1965) Intermediate states in the precipitation of hydroxyapatite. *Nature*, 23: 365–367.
5. Boskey, A.L. and Posner, A.S. (1973) Conversion of amorphous calcium phosphate to microcrystalline hydroxyapatitie. A pH-dependent, solution-mediated, solid-solid conversion. *Phys, J. Chem.*, 77 (19): 2313–2317.
6. Meyer, J. and Eanes, E.D. (1978) A thermodynamic analysis of the secondary transition in the spontaneous precipitation of calcium phosphate. *Calcified Tissue Research*, 25 (3): 209–216.
7. Harries, J.E., Hukins, D.W.L., Holt, C., and Hasnain, S.S. (1987) Conversion of amorphous calcium phosphate into hydroxyapatite investigated by EXAFS spectroscopy. *J. Crystal Growth*, 84 (4): 563–570.
8. Kivrak, N. and Tas, A.C. (1998) Synthesis of calcium hydroxyapatite – tricalcium phosphate (HA-TCP) composite bioceramic powders and their sintering behavior. *J. American Ceramic Soc.*, 81 (9): 2245–2252.
9. Seckler, M.M., Danese, M., Derenzo, S., Valarelli, J.V., Giulietti, M., and Rodrigues-Clemente, R. (1999) Influence of process conditions on hydroxyapatite crystallinity obtained by direct crystallization. *Materials Research (Sao Carlos, Brazil)*, 2 (2): 59–62.
10. Rodriguez-Lorenzo, L.M. and Vallet-Regi, M. (2000) Controlled crystallization of calcium phosphate apatites. *Chem. Mater.*, 12: 2460–2465.
11. Salahi, E. and Moztarzadeh, F. (2001) Composition of calcium phosphates precipitated from acquous solutions at different pH values. *Ceramic Forum International/Ber. DKG*, 78 (3): E43–E46.
12. Liu, C., Huang, Y., Shen, W., and Cui, J. (2001) Kinetics of hydroxyapatite precipitation at pH 10 to 11. *Biomaterials*, 22: 301–306.
13. Torrent-Burgues, J. and Rodriguez-Clemente, R. (2001) Hydroxyapatite precipitation in a semibatch process. *Crystal Research and Technology*, 36 (8–10): 1075–1082.
14. Petrov, O.E., Dyulgerova, E., Petrov, L., and Popova, R. (2001) Characterization of calcium phosphate phases obtained during the preparation of sintered biphase Ca-P ceramics. *Materials Letters*, 48 (3–4): 162–167.
15. Shuk, P., Suchanek, W.L., Hao, T., Gulliver, E., Riman, R.E., Senna, M., TenHuisen, K.S., and Janas, V. (2001) Mechanochemical-hydrothermal

preparation of crystalline hydroxyapatite powders at room temperature. *Mat, J. Res.*, 16 (5): 1231–1234.
16. Gomez-Morales, J., Torrent-Burgues, J., Boix, T., Fraile, J., and Rodrigues-Clemente, R. (2001) Precipitation of stoichiometric hydroxyapatite by a continuous method. *Cryst. Res. Technol.*, 36: 15.
17. Kim, W.S., Yano, F., Kim, W.S., and Hirasawa, I. (2002) Crystallinity of hydroxyapatite produced by reaction crystallization at low temperature. *Chem. Eng.Transac.*, 1: 611–616.
18. Sarig, S. and Kahana, F. (2002) Rapid formation of nanocrystalline apatite. *Journal of Crystal Growth*, 237–239: 55–59.
19. Raynaud, S., Champion, E., Bernache-Assollant, D., and Thomas, P. (2001) Calcium phosphate apatites with variable Ca/P atomic ratio II. Calcination and sintering. *Biomaterials*, 23 (4): 1073–1080.
20. Koumoulidis, G.C., Trapalis, C.C., Sdoukos, A.T., and Vaimakis, T.C. (2003) Preparation of hydroxyapatite nanoparticles using a modified precipitation method. *NATO Science Seriers*, 2 (102): 83.
21. Saeri, M.R., Afshar, A., Ghorbani, M., Ehsani, N., and Sorrell, C.C. (2003) The wet precipitation process of hydroxyapatite. *Materials Letters*, 57: 4064–4069.
22. Arifuzzaman, S.M. and Rohani, S. (2004) Experimental study of brushite precipitation. *J. Crystal Growth*, 267: 624–634.
23. Jenkins, R. and Snyder, R.L. (1996) *A series of monographs on analytical chemistry and its application*, : 138.
24. Wiles, D.B. and Young, R.A. (1982) Profile shape functions in Rietveld refinements. *J. Appl. Crystallog.*, 15 (4): 430–438.
25. King, P.L., Ramsey, M.S., and Swayze, G.A. (2004) Laboratory Fourier transform infrared spectroscopy methods for geologic samples. *Short Course Series-Mineralogical Association of Canada*, 33: 57–91.
26. Al-Qasas, N.S. (2004) Synthesis and Characterization of hydroxyapatitie. M.E.Sc. Thesis.
27. Riman, R.E., Suchanek, W.L., Byrappa, K., Chen, C.W., Shuk, P., and Oakes, C.S. (2002) Solution synthesis of hydroxyapatite designer particulates. *Solid State Ionics*, 151: 393–402.
28. Genck, W.J. and Larson, M.A. (1972) Temperature effects of growth and nucleation rates in mixed suspension crystallization. *AIChE Symposium Series*, 68 (121): 57–66.
29. Mathew, M., Brown, W.E., and Schroeder, L.W. (1988) Crystal structure of octacalcium bis(hydrogenphosphate) tetrakis(phosphate) pentylhydrate, $Ca_8(HPO_4)_2(PO_4)_4 \cdot 5H_2O$. *Journal of Crystallographic and Spectroscopy Research*, 18 (3): 235–250.